Heliyon 7 (2021) e06872

Contents lists available at ScienceDirect

Heliyon

journal homepage: www.cell.com/heliyon

Research article

Processing and interpretation of full tensor gravity anomalies of Southern Main Ethiopian Rift

Bisrat Kebede [a,b,*], Tilahun Mammo [a]

[a] School of Earth Science, Addis Ababa University, P.O. Box 1176, Addis Ababa, Ethiopia
[b] Ministry of Mines and Petroleum, P.O. Box 486, Addis Ababa, Ethiopia

ARTICLE INFO

Keywords:
Full tensor gravity
Tilt angle map
Gravity
Upward continuation
Basins
Structures
Tilt angle
Depth estimation
Targeting

ABSTRACT

The study area is situated in the Southern Main Ethiopian Rift being bounded within the limit of 37°00′0′-38°50′00″E and 5°50′00″-7°00′00″N. It is well known that the complex geological structure of the Main Ethiopian Rift has attracted intense attention so far and numerous geophysical investigations have been performed using potential field data-sets in Central and Northern Main Ethiopian Rift with the exception of the Southern Main Ethiopian Rift which is poorly constrained. Analysis of Full Tensor Gravity anomalies helps in understanding of the nature of shallow subsurface structural features and has a paramount importance in building general understanding of subtle details about subsurface geology of the area.

Separation of regional and residual gravity field is performed using upward continuation filtering technique. The residual gravity anomaly caused by local structures and anomalous body delineated four sub-basins with low amplitude response which is in agreement with the vertical gravity gradient anomaly (G_{zz}) and tilt derivative horizontal (TDX) that clearly outlined and characterize edges of the sub-basins. The sub-basins delineated are the northern and southern Abaya, Chamo and Gelana basins. The tilt angle method which is used to delineate major subsurface structures and determine the source depth results showed that the area was affected by different lineament trending NE-SW, N–S, NNE-SSW, NW-SE and E-W, directional analysis performed indicates that the dominant trend is in agreement with the regional fault orientations. The estimated depth to the top of the lineaments on average varies from 0.9 km to 3.1 km and it is relatively deeper in the basins compared to the surrounding areas giving clues to the amount of sediment infill.

1. Introduction

The Main Ethiopian Rift (MER) forms the incipient plate boundary between Nubia and Somalia, whose relative motion is ~95°N–100°E at rates of 4–6 mm/yr (Fernandes et al., 2004). It extends for about 500 km from the southern edge of the Afar depression in the north to the Turkana depression in the south, where it interacts with the N–S trending Kenyan rift (Ebinger et al., 2000). The rift is composed of three main segments (northern, central, and southern MER), these segments are separated by roughly E-W trending transverse structures, namely, the Yerer-Tullu Wellel volcano tectonic lineament (YTVL) (Abebe et al., 1998) between the northern MER and the central MER and the Goba-Bonga lineament (Abbate and Sagri 1980) separating the central MER from the southern MER. Both are characterized by the alignment of normal faults and major volcanoes.

Since the MER is tectonically active it attract many scholars around the world, due to this reason several geophysical and geological works have been found in public domain by different Authors. Among different geoscientific studies performed in MER, geological field studies and Remote Sensing (Satellite Imagery) are used to delineate surface structures and tectonic elements, where as to investigate subsurface structures and tectonic sittings numerous geophysical studies have been undergone. However unlike the northern and central MER (NMER & CMER), in which numerous geophysical investigations have been performed, no detail geophysical studies are conducted in the southern MER (SMER) that can constrain the geological studies conducted in this area.

This paper attempts to fill the gap and investigate the shallow subsurface geology and structural features in some detailed frame work by interpreting and correlating the Full Tensor Gravity Gradiometry (FTG) anomalies with the geology of the region. The FTG differs from conventional gravity (Ground and airborne Gravimetry) in that 5

* Corresponding author.
E-mail addresses: kbisrat79@gmail.com, kbisrat50@yahoo.com (B. Kebede).

https://doi.org/10.1016/j.heliyon.2021.e06872
Received 27 September 2020; Received in revised form 14 November 2020; Accepted 16 April 2021
2405-8440/© 2021 The Author(s). Published by Elsevier Ltd. This is an open access article under the CC BY-NC-ND license (http://creativecommons.org/licenses/by-nc-nd/4.0/).

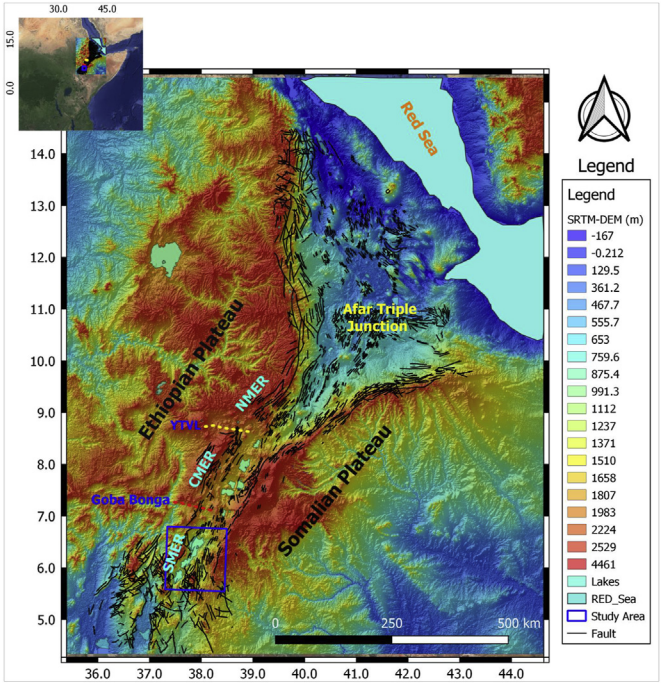

Figure 1. Ethiopian Rift system, Shuttle Radar Topography Mission (SRTM) digital elevation model: 30 m resolution, Faults extracted from geological map of Ethiopia (Mengesha et al., 1996).

independent components (G_{xx}, G_{yy}, G_{xy}, G_{xz}, and G_{zz}) of the Gravity gradient field are recorded during underway surveys (Murphy 2004). Gravity anomalies are the cumulative result of the interferences of geological sources with different shape, densities and depths. Of particular interest to a structural geologist is the linear anomaly in geophysical maps which may correspond to buried faults, contacts, and other tectonic and geological features. FTG, Ground and airborne Gravimetry methods are used worldwide for detection of these structures and determination of the depth of the anomaly sources is one of the main aims of quantitative interpretation of gravity field map.

Full Tensor Gravity Gradiometry (FTG) measures the derivative of all the three gravity components in all three directions and provides a rich source of information for defining edges of geological structures at both local and regional scales (Dickinson et al., 2010). Murphy (2004) describes the five components of FTG; G_{xx}, G_{xy}, G_{yy}, G_{xz} and G_{yz}, and the vertical component G_{zz} and discusses how they provide valuable information for the mapping of subsurface geology. FTG has proven to be an effective tool in oil, gas and mineral exploration (Dickinson et al., 2012). Analysis of Full Tensor Gravity Gradiometry (FTG) anomalies helps to understand the nature of structural features with their estimated depth and has a paramount importance to better characterize the geology.

A more accurate approach when working with the Tensor components is to treat them as a collective entity. The tilt angle method (TAM) combines the horizontal and vertical components of FTG data and then used to map geological trends with its associated estimated depth. Edge detection and source depth estimations are common routines in the potential field studies and play important role in detecting faults. The techniques are based on the adaptive tilt angle method (ATAM) obtained from the three independent Full Tensor Gravity Gradiometry (FTG) anomalies G_{zz}, G_{zx} and G_{yz} (Salem et al., 2011) and tilt angle method (TAM) computed from analytic signal from tensor components G_{xx}, G_{yy} and G_{zz} in order to compare and contrast the results and better characterize the tectonics and geology of the study area.

In this paper an attempt is made to delineate the geological structures and rift basin architecture of the southern main Ethiopian rift using tilt angle method derived from the independently measured FTG components and interpretation of the Bouguer gravity anomaly.

2. Geological setting of the study area

The Main Ethiopian Rift (MER) has a complex structural pattern composed of southern, central, and northern segments. Ages of onset of faulting and volcanism apparently indicate a heterogeneous time-space evolution of the segments, generally referred to as a northward progression of the rifting process (Bonini et al., 2005). The pre-rift flood--basalt event of the Southern MER is dated back to 45 Ma; this indicates that in the Southern MER the Tertiary rift system is started earlier than Central and Northern MER (Davidson and Rex, 1980; George et al., 1998; WoldeGabriel et al., 1991; Yemane et al., 1999; Ebinger et al., 2000). The major fault escarpments characterized the Southern MER are the

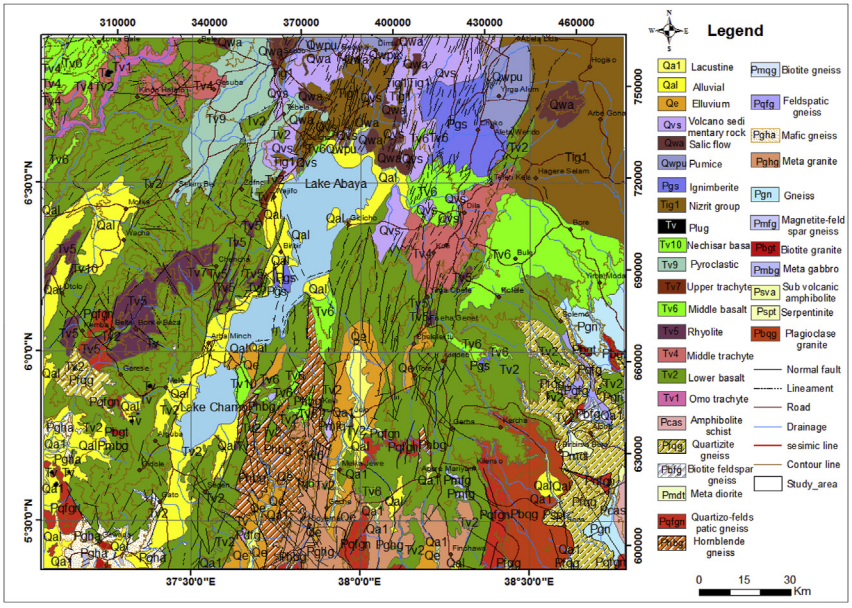

Figure 2. Geological map of Southern Main Ethiopian Rift modified from Geological Map of Dilla and Ageremariam map sheets, scale 1:250,000, compiled by the Geological Survey of Ethiopia (Yismaw et al., 2015) and (Gebriel et al., 1997) respectively.

Chencha (western margin) represents the alternating opposed major border fault 60 km and the Agere Selam (eastern margin) where the northern end of this border fault is truncated by the Bonga lineament (Woldegabriel et al., 1990). The southern sector of the Main Ethiopian Rift is divided into two Chamo basin to the west and Galana basin to the east by Amaro Horst, highly elevated Precambrian basement having a length of ~90 km (Levitte et al. 1974; Ebinger et al., 1993). The structures of Southern MER have N–S trends in Amaro Horst and Galana basin, whereas the structural patterns of Chamo basin shows alternative trends from NW–SE to NE– SW (Corti 2009). Structural analysis of fault slip data carried out by Bonini et al. (2005) on the Chencha escarpment-Lakes Abaya and Chamo indicate a poly phase deformation associated with different episode of rifting.

Geological cross section measured in the field by Ebinger et al. (1993) from Lake Chamo to Gelana basin via Amaro horst shows that Gelana basin is associated with an asymmetric architecture in which the total sediment thickness may exceed ~4 km and a symmetric structure in Chamo basin with syn-rift thickness reaching ~2 km, however gravity modeling conducted by Mahatsente et al. (1999) does not confirm the result obtained from the geological studies concerning the asymmetric structure in this rift segment. Since there are only few geophysical studies in the area, the subsurface structures and sediment infill thickness of Southern MER are poorly constrained and inference is made only from the geological field and enormous geophysical studies conducted on Central and Northern MER. Geophysical investigations on Central MER by Le Turdu et al. (1999) estimated the presence of about 600 m of Late Cenozoic fluviolacustrine sediment. Similar fluviolacustrine sediments with a thickness exceeding 500 m delineated in Abaya and Chamo Lake basins of southern MER by Ebinger et al. (1993), which is also not constrained. The lakes in the MER today are only remnants of more extensive Plio-Pleistocene lakes stretching from Awash basin in the north up to Abaya-Chamo Lakes in the south until it separated into the present lakes by Late Pleistocene tectonic movements (Tiercelin and Lezzar 2002): for example, the Lower Pliocene Chorora Formation was deposited in a lake covering over 1000 km^2 (Sickenberg and Schönfeld 1975). Pleistocene-Holocene lacustrine sediments cover a significant tract of ground and were deposited in a huge lake whose level before 3500 to 2100 years used to be 100 m higher than its current level (Kazmin et al., 1980). It is reasonable to postulate, therefore, that extensive lakes might have been present in the MER during the Paleogene, with deep anoxic waters where algal and other organic matter was preserved and the high heat flow rates associated with the rift valley could have generated oil from any such source rocks.

There has been no significant exploration for oil and gas deposits in the Main Ethiopian Rift. In fact, the intense associated volcanism, with inferred high temperatures, has been seen historically as detrimental to any hydrocarbon potential. Subsurface temperatures measured in the MER reveal 270 °C at 1000 m at Aluto/Langanno and 315–335 °C at 2200 m at Tendaho in the MER/Afar transition (Abebe 2000). Such temperature levels, if widespread, will have destroyed most of any oil generated as well as any porosity and permeability in sandstone and carbonate units. However, both these hydrothermal exploration wells targeted known 'hot-spots' in the rift, and the high temperatures encountered should not be generalized over the entire rift. It may be, for instance, that the higher temperatures and intrusions are concentrated along the Wonji Fault Belt (Mohr 1967) and that elsewhere within the rift there are relatively cool, un-intruded areas that have oil potential. Since no detailed geophysical studies are available, the subsurface rift architecture in the Southern MER remains poorly constrained, thus only future investigation of the rift subsurface can address that uncertainty.

3. Gravity data and data processing

In 2013, Africa Oil Ethiopia B.V entered into Petroleum Production Sharing Agreement with the government of Ethiopia to explore oil and gas in the rift basin block of central Ethiopia. The Company completed 30,506 km^2 Full Tensor Gravity Gradiometry survey in southern and central main Ethiopian Rift valley basins block (Africa Oil Corp 2013a). Data was acquired using a full tensor FTGeX gravity gradiometry system from Lockheed-Martin with a Resolution or target sensitivity of 1E/$\sqrt{}$Hz (Difrancesco 2007). The FTGeX instrument also includes direct measurement of the vertical gravity signal via the Gravity Measurement Assembly (GMA). The survey was planned and acquired with line spacing of 1000 m and Tie line spacing of 5000m; with accelerometer bias not varying more than 500 micro-g. The survey was designed/flown to follow the terrain at a nominal height of 120 m above ground level as shown below (Figure 3). Data was not collected over the entire length of the Amaro Horst (~90 km) since it is a Precambrian basement with no hydrocarbon prospect. Nevertheless, a good portion of it (~70 km) is still

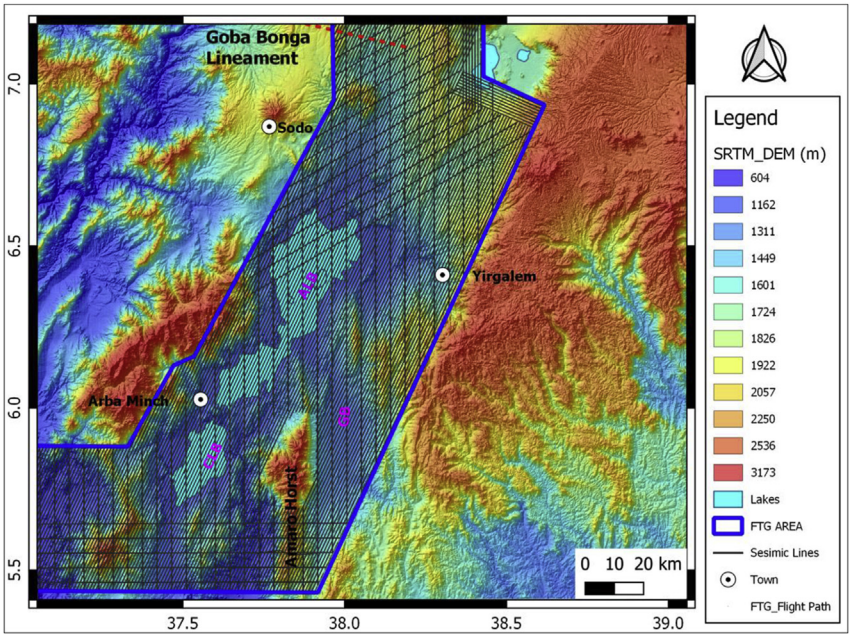

Figure 3. Location of the FTG flight path on SRTM digital elevation model: ALB = Abaya Lake Basin, CLB = Chamo Lake Basin and GB = Gelana Basin.

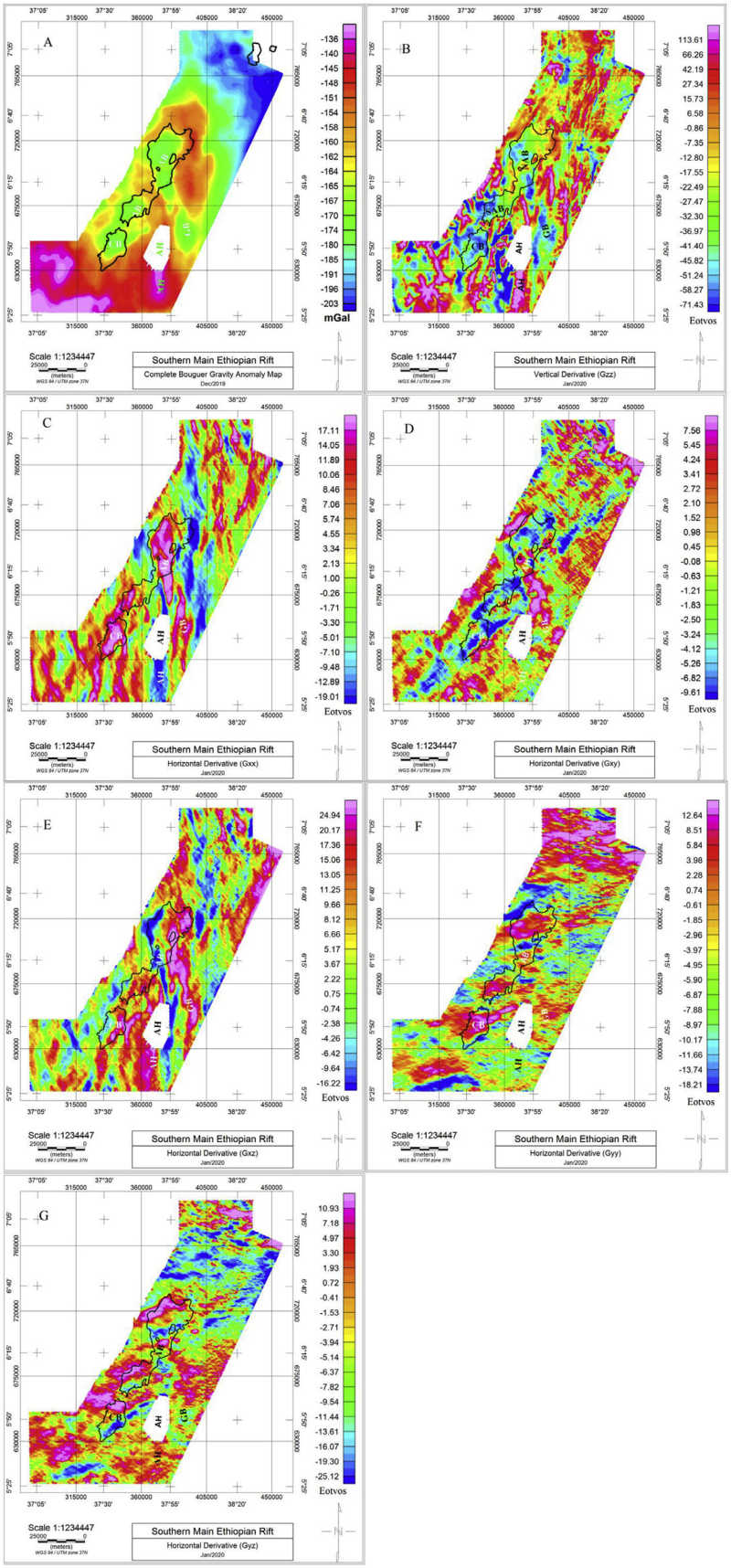

Figure 4. Vertical gravity signal (GMA) and FTG Components: A = Complete Bouguer Anomaly Map, B = G_{zz}, C = G_{xx}, D = G_{xy}, E = G_{xz}, F = G_{yy} and G = G_{yz},: AB = Abaya Basin, CB = Chamo Basin, GB = Gelana Basin, and AH = Amaro Horst; the overlapped polygons are Abaya and Chamo Lake shape files. Gravity Gradients are measured in units of Eötvös, with 1 Eötvös equal to 0.1 mGal/km.

covered to maintain continuity with the adjacent areas. The upper central part remains unsurvey as indicated in a FTG flight path map (Figure 3) as an empty space. In all the data processing steps this gap in data is retained without performing any interpolation.

The FTG data processing including self-gradient correction, Post Mission Correction (PMC), leveling, equivalent source (ES) processing and de-noising were performed, the G_{zz} and g_z micro-levelled grids were produced by removing the residual line and tie line noise and the complete set of gravity gradient components in the geographic frame was computed from the micro-levelled vertical gravity gradient G_{zz} grids and the resulting grids G_{xx}, G_{yy}, G_{xy}, G_{xz} and G_{zz}, those processing were done using ARKeX proprietary software (McBarnet 2004).

The Gravity Measurement Assembly (GMA) corrections: the vertical acceleration, Eotvos, drift, latitude, tide, and free-air were calculated using Geosoft Oasis Montaj's gravity processing package (Montaj 2015). The final corrected Free-Air GMA was further filtered with a 250 s Gaussian low pass filter and is corrected for the variation of the terrain by removing the signal of the land body using a specified density and removing the combined signal of the Water bodies (assumed a value of 1g/cc). This effectively removes the signal from the land and the water column. This correction was applied with a density value of 2.5 g/cc, which was chosen after comparing different values using a Nettleton test (Africa Oil Corp 2013b).

In this paper about 16,500 km^2 of the micro leveled full tensor gravity gradient and vertical gravity terrain corrected grids at a drape are being used for further processing and interpretation to delineate the structural fabrics and the architecture of the southern main Ethiopian rift basin.

4. Methods

Analysis and interpretations of full tensor gravity (FTG) as well as vertical gravity signal from gravity measurement assembly (GMA) are carried out; a complete Bouguer gravity and the FTG components G_{xx}, G_{xy}, G_{yy}, G_{xz}, G_{yz} and G_{zz} anomaly maps of the study area was produced with a grid spacing of 72.0 m × 72.0 m (Figure 4).

5. Separation of regional and residual field

The anomalous value of the gravity field at a point is the sum of the gravity effects of widespread and deep-seated mass distributions and smaller, localized mass distributions near the observation point. The interpretation of Bouguer gravity anomalies often involves isolating anomalies of interest (residual gravity anomalies) (Mickus et al., 1991). The observed Bouguer gravity anomaly field consists of two components: a regional and residual gravity anomaly field. Since the study presented herein deals with the shallow geological structures and rift basin architectures of the southern main Ethiopian rift, regional/residual separation process was applied to gravity data-set in order to estimate the amplitude of the regional background.

Upward continuation can be used to separate a regional gravity anomaly resulting from deep sources from the observed gravity (Kebede et al., 2020; Mammo 2013). This is an operation that shifts the data by a constant height level above the surface of the earth (or the plane of measurements). It is used to estimate the large scale or regional (low frequency or long wave length) trends of the data.

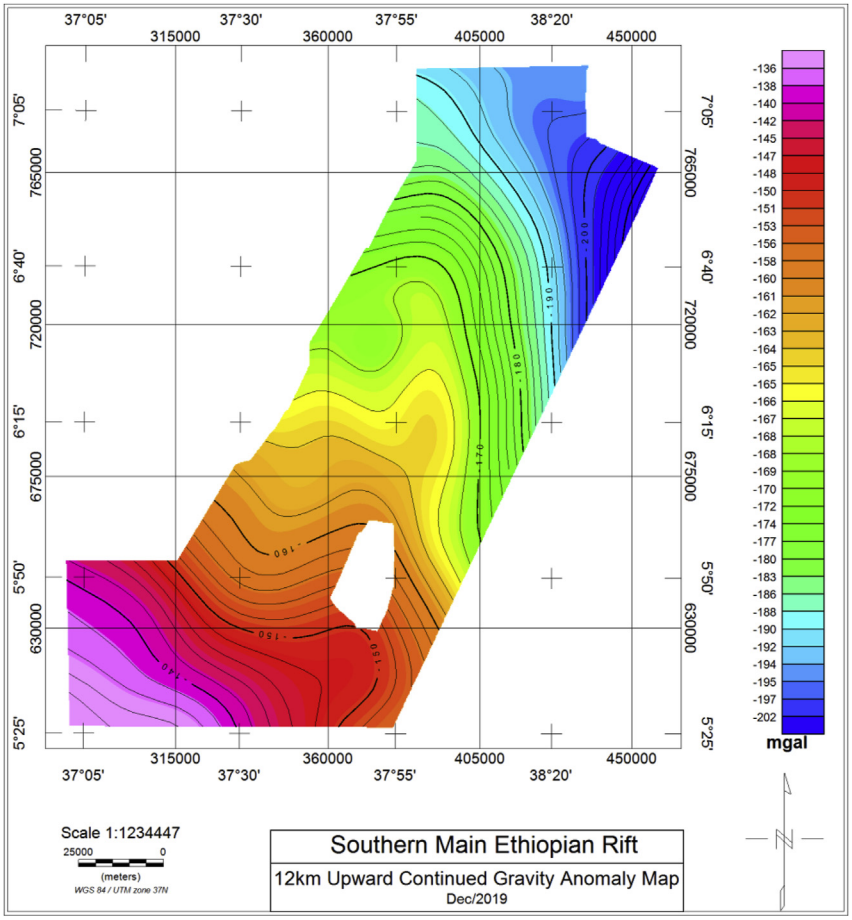

Figure 5. Regional gravity background of the study area computed by upward continuation filter. Contour interval: 2 mGal.

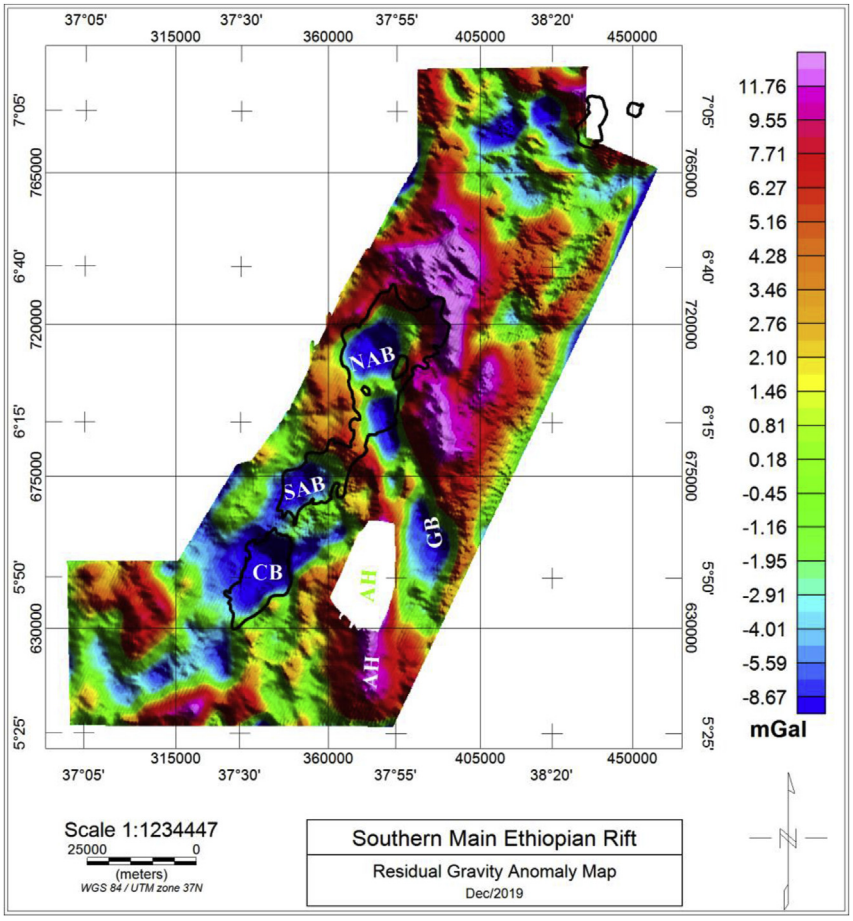

Figure 6. Residual gravity anomaly map: NBA = Northern Abaya Basin, SBA = Southern Abaya Basin, CB = Chamo Basin, GB = Gelana Basin and AH = Amaro Horst; the overlapped polygons are Abaya and Chamo Lake shape files.

Since the target depth is the basement which is approximately undulating 5 km–6 km, the data is upward continued at 12 km to remove the short wavelength anomalies. Jacobsen (1987) demonstrated that if a potential field is upward continued to a certain height z, then it is possible to focus on sources situated at a depth greater than $z/2$ (see also Lyngsie et al., 2006; Mammo 2010).

The residual gravity anomaly (Figure 6) is computed by removing the regional (Figure 5) effect from the complete Bouguer gravity anomaly (Figure 4A).

6. Edge detection and depth estimation using tilt angle

The tilt angle is the angle computed as the arctangent of ratio of the first vertical derivative to the first horizontal derivatives of the gravity field. Its parameter varies between $-\frac{\pi}{4}$ and $+\frac{\pi}{4}$ where the zero contours locate close to the source-body contact.

Miller and Singh (1994) developed the tilt angle filter (θ) described in Eq. (1) shown below.

$$\theta = \tan^{-1}\left(\frac{\frac{\partial M}{\partial z}}{\sqrt{\left(\frac{\partial M}{\partial x}\right)^2 + \left(\frac{\partial M}{\partial y}\right)^2}}\right) \quad (1)$$

where θ is Tilt angle Filter, M is the gravity or magnetic field and $\frac{\partial M}{\partial z}$, $\frac{\partial M}{\partial x}$ and $\frac{\partial M}{\partial y}$ are the first derivatives of the field M in the x, y and z directions.

The tilt amplitudes are restricted to values between $-\frac{\pi}{2}$and $+\frac{\pi}{2}$ according to the nature of the arctangent trigonometric function and respond to a large dynamic range of amplitudes for anomalous sources at the different depths. Its amplitude has three rates: positive over the source, zero at or near the edge of the source, and negative outside the source (Ibraheem et al., 2018). In the presence of noise, this technique acts as an effective signal discriminator for both shallow and intermediate sources but becomes blurred for sources at considerable depths, where it can not reveal deep-level geologic boundaries (Arisoy and Dikmen 2013).

This technique can be used to estimate depth of the upper end of vertical contact source obtained by measuring the perpendicular distance between contours $\theta = 0^0$ and $\theta = \pm\frac{\pi}{4}$. The distance between zero and $\pm\frac{\pi}{4}$ pairs obtained from the tilt angle map corresponds to the depth to the top of the vertical contact model. Alternatively, the half distance between $-\frac{\pi}{4}$ and $+\frac{\pi}{4}$ radians is equal to the depth to the same model. It can easily be calculated from the reciprocal of horizontal gradient values at the zero contour points. The zero contours estimate the location of abrupt lateral changes in density of basement materials.

7. Adaptive tilt angle (ATA)

Full Tensor Gravity Gradiometry (FTG) accurately maps subsurface density contrasts caused by target geology, and simultaneously maps their geological structures. However, FTG Gravity data are often underused due to an over reliance on interpreting the vertical gravity gradient anomaly G_{zz} component with little consideration given to horizontal component data (Murphy and Dickinson 2010). Murphy (2007) and

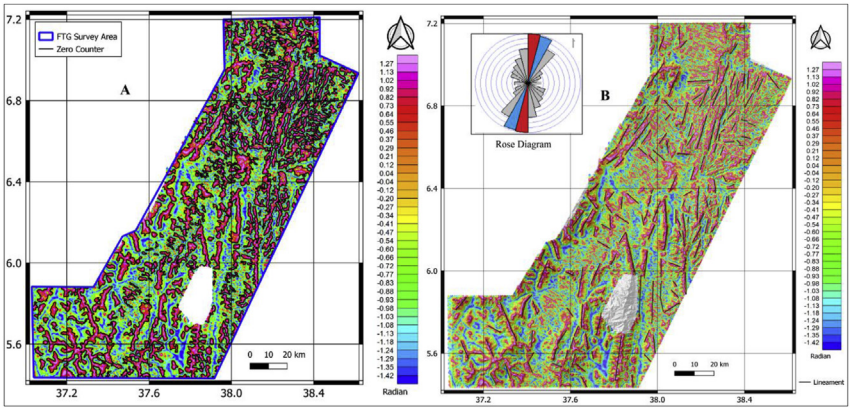

Figure 7. (A) The computed adapted tilt angle with ($a = 1$) for vertical contact, black lines show 0° contours, which indicate the enhanced related structures of the Southern Main Ethiopian Rift. (B) ATA with extracted lineament: the Rose diagram highlighting the orientations of the main trend displayed on SRTM-DEM hill shade.

Murphy and Brewster (2007) describe a procedure for working with Gravity Gradient Tensor data, they demonstrate that combining all, or partial sets, of Tensor components into new Tensor representations, facilitate identification of sub-surface geological complexity in terms of shape, size and orientation of target structures.

Although there are five independent components in the full tensor gravity data set at each observation point, it is important to note that they are all linearly related to the underlying gravity potential. Due to this reason an interpretation of individual tensor components also leads to under usage of the full tensor gravity data. A more accurate means of working with Tensor components is to treat them as a collective entity. One such method that combines the three full tensor gravity data sets G_{zz}, G_{xz} and G_{yz} is that first described by Salem et al. (Salem et al., 2011).

The Adaptive Tilt Angle Method described by Salem et al. (2011) and how it is used for FTG data and he defines the Adaptive Tilt Angle (θ_a) as:

$$\theta_a = \tan^{-1}\left[a\frac{G_{zz}}{\sqrt{{G_{xz}}^2 + {G_{yz}}^2}}\right] \tag{2}$$

where a is a value characterizing the source type, it is, in essence, a structural index like that adopted for Euler Deconvolution methods, θ_a is Adaptive Tilt Angle Filter and G_{zz}, G_{xz} and G_{yz} are the measured FTG data components (Figure 4).

Using Eq. (2), the following Eqs. (3), (4), (5), and (6) are derived by Salem et al. (2011) for estimating the location and depth of simplified geometric targets from FTG data as shown below.

$$\theta_a = \tan^{-1}\left[\frac{2{z_o}^2 - h^2}{z_0|h|}\right] \text{ For point mass } (a = 3). \tag{3}$$

$$\theta_a = \tan^{-1}\left[\frac{{z_o}^2 - h^2}{2z_0|h|}\right] \text{ for horizontal line of mass } (a = 1). \tag{4}$$

$$\theta_a = \tan^{-1}\left[\frac{z_0}{|h|}\right] \text{ for vertical sheet } (a = 1). \tag{5}$$

$$\theta_a = \tan^{-1}\left[\frac{h}{z_0}\right] \text{ for horizontal sheet } (a = 1). \tag{6}$$

where θ_a is ATA, h is the horizontal distance from the source and z_0 is the depth to the source.

The tilt angle produces a zero value over the source edges and, therefore, can be used to trace the outline of the edges (Miller and Singh 1994). The zero contours of the tilt angle correspond to the boundaries of geologic discontinuities and are used to detect the linear features in the full tensor gravity data. Following the linear trends of the zero contours on the tilt derivative map of the study area lineaments are extracted as shown in below (Figure 7A & B).

8. Tilt angle (TA) using analytic signal

Beiki (2010) used an analytic signal approach applied to FTG data to estimate the source location parameters of simple gravity bodies. The disadvantage of the analytic signal approach is that it is more sensitive to noise than conventional approaches.

In this paper another tilt angle is computed using the analytic signal generated from the full tensor gravity data components G_{zz}, G_{xx} and G_{yy} (Figure 4), in order to get better structural features of the area by comparing and contrasting the results from earlier adaptive tilt angle anomaly signatures.

The analytic signal map was generated from full tensor gravity (FTG) components using Eq. (7) as shown below.

$$|As(x,\ y, z)| = \sqrt{\left({G_{xx}}^2 + {G_{yy}}^2 + {G_{zz}}^2\right)} \tag{7}$$

where $|As(x,\ y, z)|$ is analytic signal magnitude and G_{xx}, G_{yy} and G_{zz} are Full Tensor gravity components (Figure 4).

The tilt angle map is generated using the analytic signal (Figure 8) as an input by tilt angle formula described in Eq. (1).

$$\theta = \tan^{-1}\left[\frac{\frac{\partial|As(x,\ y,z)|}{\partial z}}{\sqrt{\left(\frac{\partial|As(x,\ y,z)|}{\partial x}\right)^2 + \left(\frac{\partial|As(x,\ y,z)|}{\partial y}\right)^2}}\right] \tag{8}$$

where θ is Tilt Angle and $|As(x,\ y, z)|$ is Analytic Signal.

Zero counters are extracted from the tilt angle map which is computed using Eq. (8) and then the lineaments are extracted from zero counters, linear features that show the various structural fabrics in the southern main Ethiopian rift (Figure 9A & B).

Directional analysis was done on the extracted lineaments of both tilt angle map displayed on SRTM-DEM hill shade on (Figure 7B & 9B) and the rose diagrams highlighting the orientations of the main trend in agreement with the regional fault orientations extracted from Ethiopian Geological Map (Figure 1) by Mengesha et al. (1996). By comparing and contrasting the lineament extracted from both Adaptive Tilt angle (θ_a)

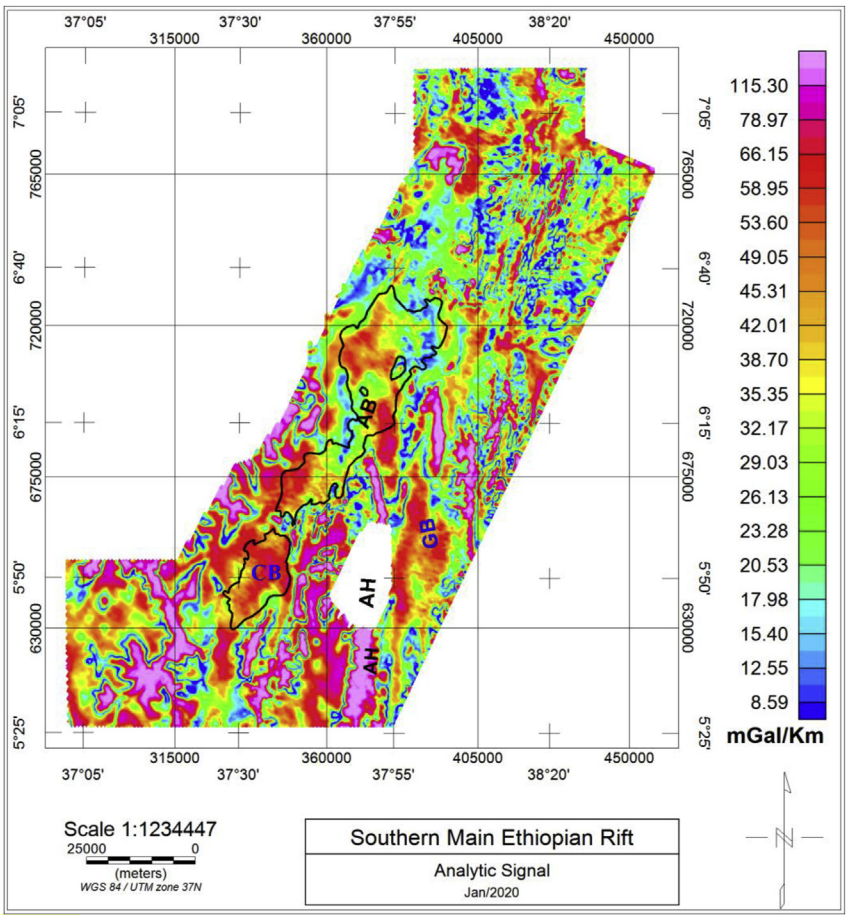

Figure 8. Analytic signal map generated using the vertical and the horizontal tensor components, AB = Abaya Basin, CB = Chamo Basin and AH = Amaro Horst; the overlapped polygons are Abaya and Chamo Lake shape files.

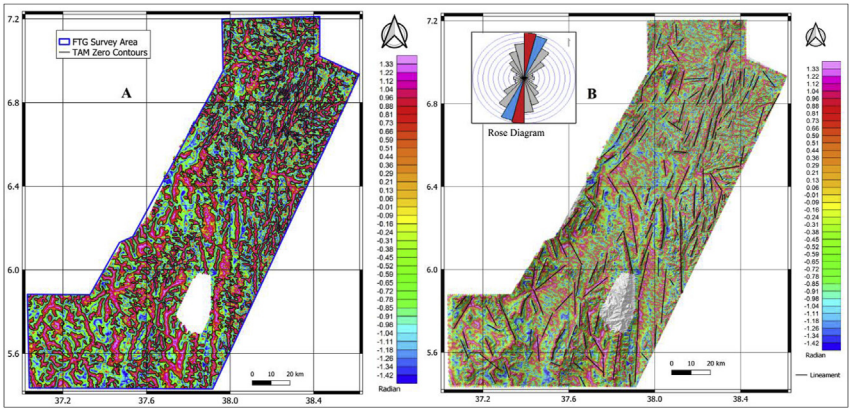

Figure 9. (A) Tilt angle map generated from Analytic Signal with zero contours. (B) TAM with extracted lineament: Rose diagram highlighting the orientations of the main trend displayed on SRTM-DEM hill shade.

and Tilt angle (θ) computed from the full tensor gravity components which have almost identical structural fabrics and linear trends as shown in (Figure 7B & 9B), the final lineament map of southern main Ethiopian rift (SMER) is generated. The result is presented with reference fault extracted from Ethiopian Geological Map (Mengesha et al., 1996) as shown in below (Figure 10).

Both the existing and the extracted lineaments are overlaid on SRTM-DEM hill shade and the directional analysis is performed using the rose diagrams highlighting the orientations of the main trends which is almost identical on both maps as shown in (Figure 10A & B).

9. Source depth estimation

The depth of the lineaments (Vertical contact) can be computed using Equation-6 for horizontal sheet ($a = 1$)which can be applied to both Adaptive Tilt angle (θ_a) and Tilt angle (θ). According to Salem et al. (2011) in the case of a thin vertical sheet, we assume that its thickness t is negligible; we therefore apply the approximation that the edges of the sheet correspond to the horizontal location of the source ($h = 0$). The depth to the edge of the horizontal sheet source corresponds to the distance between 0^o and 45^o adaptive tilt angle values ($h = z_c$); this result

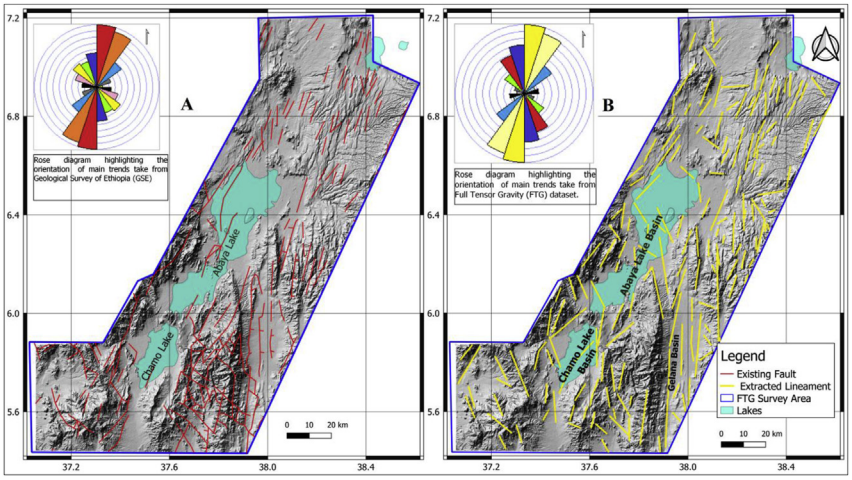

Figure 10. (A) Existing faults extracted from the Geological map of Ethiopia (Mengesha et al., 1996). (B) Extracted lineament using full tensor gravity data set displayed on SRTM-DEM hill shade.

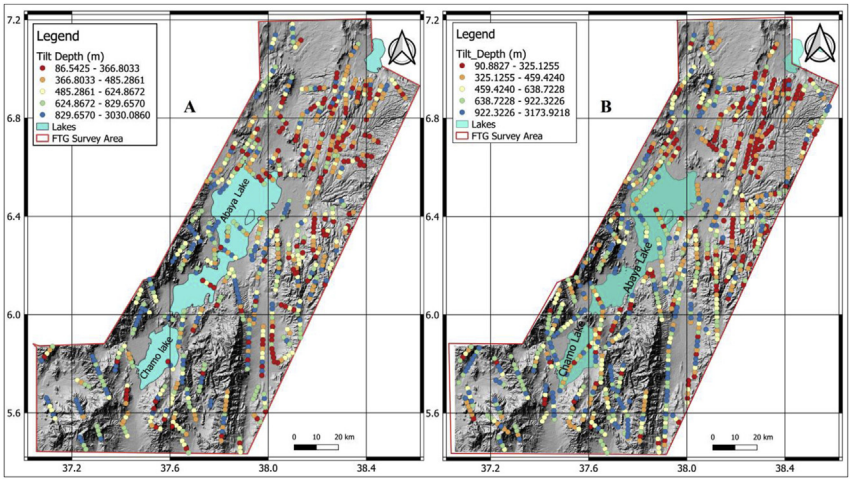

Figure 11. (A) Tilt Depth extracted from adaptive tilt map prepared by G_{zz}, G_{xz} and G_{yz}. (B) Tilt Depth extracted from tilt map prepared from analytic signal using G_{zz}, G_{xx} and G_{yy} displayed on SRTM-DEM hill shade.

is similar to vertical contacts from magnetic data described by Salem et al. (2007) shown below;

$$\theta = \tan^{-1}\left[\frac{h}{Z_c}\right] \tag{9}$$

where h is the horizontal distance from the source, θ tilt angle and z_c is the depth to the contact. Equation-9 indicates the value of the tilt angle above the edges of the contact is 0^o ($h = 0$) and equal to 45^o when $h = z_c$ and -45^o when $h = -z_c$. This suggests that contours of the tilt angle can identify both the location at ($\theta = 0^\circ$) and depth (half the physical distance between $\pm 45^o$contours) of contact-like structures.

Thus, the mapped shape of the zero contours indicates the mapped shape of the causative source, and the horizontal distance between the zero and $\frac{\pi}{4}$ contours provides an estimate of the depth to the top of the linear trends beneath the zero contours. The tilt angle map computed from the full tensor gravity components is a very useful interpretation tool since it provides a simple and clean image. The technique tends to enhance mapping of the subtle gravity anomalies, and maximizes characterizing the geometrical contrast of the anomalous sources and the method produces satisfactory depth estimation.

In this paper depth estimation is performed on both Adaptive Tilt Angle and Tilt Angle as shown in (Figure 11A & B). The depth estimated on average varies from 0.9 km to 3.1 km. Most of the shallow depth linear trends are observed in the northern parts of the area and only few shallow depth linear trends are observed on the central parts, that is, the depth of the linear trends observed in the Abaya, Chamo Lake and Gelana basins are relatively deeper compared to the surrounding study areas.

10. Automatic edge detection on tilt derivative horizontal (TDX)

Tilt Derivative Horizontal (TDX) proposed by Cooper and Cowan (2006) is the amplitude of the horizontal gradient that is normalized to the absolute value of the vertical derivative. It can be computed by Eq. (10) as follows:

$$TDX = \tan^{-1}\left(\frac{\sqrt{\left(\frac{\partial M}{\partial x}\right)^2 + \left(\frac{\partial M}{\partial Y}\right)^2}}{\left|\frac{\partial M}{\partial z}\right|}\right) \tag{10}$$

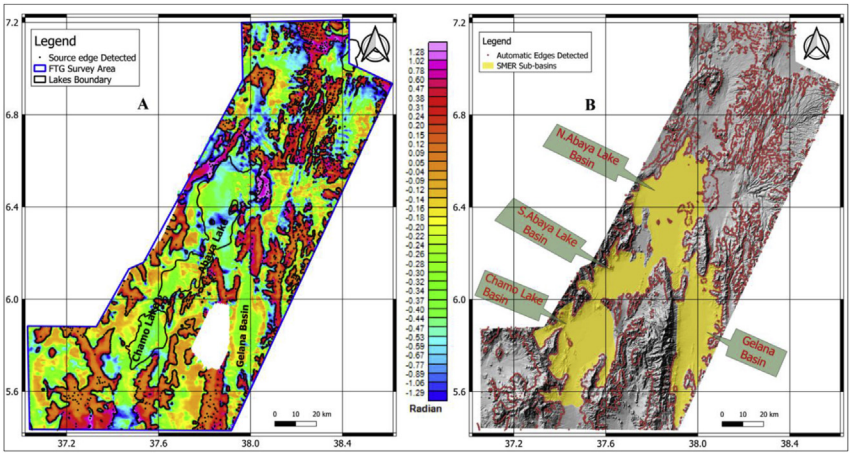

Figure 12. (A) Tilt Derivative Horizontal (TDX) generated from G_{zz}, G_{xz} and G_{yz}. (B) target area delineated for further geoscience investigation displayed on SRTM-DEM hill shade.

where *TDX* Tilt Derivative Horizontal Filter, M is the gravity or magnetic field and $\frac{\partial M}{\partial z}$, $\frac{\partial M}{\partial x}$ and $\frac{\partial M}{\partial y}$ are the first derivatives of the field M in the x, y and z directions.

The positive peak values in Tilt Derivative Horizontal (TDX) grid are then extracted to locate the source edges using an automatic edge detection method. Tilt Derivative (TDR) works effectively with data from shallow sources, but it is considered relatively ineffective when dealing with data from deep sources. TDX is the inverse of the TDR proposed; as it performs equally well with both shallow and deep sources. Horizontal Tilt Derivative (TDX) (Figure 12A) is generated from the inverse of the tilt angle map prepared from G_{zz}, G_{xz} and G_{yz} (Figure 4) and an automatic edge detection performed on TDX clearly outlined the sub-basins edges. Target area is also delineated using overall full tensor gravity data interpretations (Figure 12B).

11. Results and discussion

The Bouguer anomaly map (Figure 4A), correlated with lateral density variations in the crust generally shows anomaly variations from minimum of -200 mGal to the maximum of -130mGal. The N–S trending high amplitude gravity anomaly zone in the southern part of the area corresponds to Amaro Horst, it separate Chamo Lake basin to the west from Gelana basin to the east and continue in the NW-SE direction parting the Abaya Lake basin at its center (Figure 4A). The high amplitude metamorphic basement signature is clearly visible covering the region in the immediate west of the Amaro Horst. High values are also observed in the central parts of the area north and east of Lake Abaya. The basin areas are characterized by relatively lower gravity value.

The residual gravity anomaly map (Figure 6) displays that the computed anomalies vary from -8mGal to +14mGal, indicating a clear gravity contrast in the area which could be regarded as sufficiently clear indicator to distinguish the effects of causative geological sources. The southern main Ethiopian rift basin architecture is clearly outlined into four sub-basins i.e., northern and southern Abaya basins, Chamo and Gelana basins. Amaro Horst, a narrow block of Precambrian basement that widens and declines southwards over a length of ~90 km (Levitte et al. 1974; Ebinger et al., 1993) shows a high gravity anomaly greater than 10 mGal. The local low amplitude gravity anomaly in (Figure 6) which is less than -8 mGal over the rift basins may be interpreted as a low density source rocks, that is, post-rift and syn-rift sediment depositions.

Considering the geological map of the study area (Figure 2), it is seen that lacustrine alluvium and eluvium are mostly prevalent at Abaya, Chamo and Gelana basins. Thus, it can be mentioned that those sedimentary units having relatively lower densities evidently contribute to the decreasing of the amplitudes of gravity anomalies at the sub-basins. The behavior of those anomaly signatures fits quite well with the surface geology map and previous geological studies of the southern main Ethiopian rift. From the geological map displays that Quaternary, Tertiary sedimentary rocks (lacustrine, alluvium, eluvium) and Late Cenozoic sedimentary rocks (fluviolacustrine) deposit associated with lower density formation were outlined in Abaya, Chamo and Gelana basins which give rise to the lowering of the gravity amplitudes. Poorly studied fluviolacustrine deposits occur in the southern MER in the Abaya/Chamo Lake regions with a thickness of more than 500 m (Ebinger et al., 1993). A local high amplitude gravity anomaly greater than 10 mGal (Figure 6) north and upper east of Abaya corresponds to volcanic sedimentary rock, Sialic and basaltic flows (Figure 2).

FTG data interpretation can be rigorous due to the complex nature of each Tensor component. However, well known procedures adopted for conventional potential field data such as wavelength filtering are routinely used to obtain a first pass qualitative interpretation. The strength of these techniques allows careful discrimination of target signature patterns promoting increased confidence in geological mapping exercises (Murphy et al., 2005). However, the techniques tend to treat the individual Tensor components as separate individual data sets and not as part of the same Gravity field. The danger of this approach is the likelihood of not being able to see the full picture and lead to misinterpretation of a signature pattern not common to all data sets. The procedure presented in this paper combines the horizontal and vertical component data and then uses these to map geological trends across the survey area imaged in vertical gravity gradient (G_{zz}) (Figure 4B), as it best characterizes geological structure and stratigraphy. So in this study little consideration is given to the interpretations of individual tensor component of the FTG because in tilt derivative all the tensor components are combined to obtain better pictures of the subsurface structures.

The horizontal FTG gradient component G_{xx} and G_{yy} (Figure 4C & F) accentuates linear trends and faults in North - South and East - West directions respectively, whereas G_{xz} and G_{yz} (Figure 4E & G) accentuates contacts and edges in North - South and East - West directions. The vertical gravity gradient components of FTG datasets G_{zz} (Figure 4B) remove the long wavelengths and preserve intermediate and short wavelengths that are essential for the study of local and relatively shallower sub-surface structures equivalent to the residual gravity anomaly map.

The vertical gravity gradient component of FTG datasets G_{zz} (Figure 4B) shows contrasting gravity gradient anomalies with the gravity values varying between -70Eotvos and +160Eotvos. In agreement with the residual gravity anomalies (Figure 6) the vertical gravity gradient G_{zz} clearly outlined the sub-basins with its low gradient

amplitude less than 40 Eotvos. Also the Amaro Horst acquires the highest gravity gradient amplitude with its shape and geometry accurately outlined (Figure 4B). The sedimentary rocks have low vertical gravity gradient anomaly (G_{zz}) and are bounded by denser volcanic and metamorphic rock which, naturally, are associated with high vertical gravity gradient anomaly (Figure 4B). Generally, the SMER is floored by high gradient anomalies. The basins are characterized by low anomalies as they are filled by thick sedimentary deposits.

Unlike the central and northern Main Ethiopian Rift, the subsurface geology of the southern rift is poorly constrained, this study highlights the key role of potential field (full tensor gravity survey) in better understands the subsurface structural features of the complex geological setting of southern main Ethiopian rift and reveal some significant geological implications and in this paper all the lineaments outlined using the FTG data sets are subsurface structures with a ranges of average estimated depth to the top of the linear trends varies from 0.9 km to 3.1 km relative to the surface (Figure 11A & B).

By comparing and contrasting the lineament extracted from the zero contours of Tilt angle maps (Figure 7B & 9B) which have almost identical linear trends, the final lineament map (Figure 10B) of (SMER) is generated and the result is presented with reference to fault map (Figure 10A) of the SMER. The directional analysis of the extracted lineaments from FTG has been done with the reference fault of map (Figure 10A). The results verify the similarity in the NE-SW, N–S and SSW - NNE trending lineaments with the exception of the NW-SE and few nearly E-W lineaments that are extracted from the FTG data (Figure 10B). The rose diagram on both maps (Figure 10A & B) highlights the orientation of the main trends in SW-NE and SSW-NNE directions along the axial portions of the main Ethiopian rift. The major trends of lineaments extracted from the FTG data have NE-SW, N–S, NNE-SSW, NW-SE and nearly E-W directions. The dominant lineaments align the axial portions of the main Ethiopian rift; the lineaments in the rift floor and the rift shoulders. The N–S to NNE-SSW active systems of faults have played important roles in forming the rift floor and the NE-SW striking faults defining the rift margin which are reactivated during the East African rifting at Neogene period generally affecting the topographic expression of the Main Ethiopian Rift (MER) and have produced an appreciable throw reaching up to 200 m (Boccaletti et al., 1998; Korme et al., 2004).

The N–S trending lineaments are dominant in Gelana basin with the master faults on the western side of the basin where the Amaro Horst resides. Previous study in correspondence to the Amaro Horst which parts Chamo basin to the west and Gelana basin to the east attain an N–S trend. The faults of the Galana Basin are linear with pure N–S trend; the structures bounding the northern Abaya, southern Abaya and Chamo basins are more segmented and characterized sharp changes in orientation from NW–SE to NE– SW (Figure 10B), as suggested by Corti (2009).

The NW-SE and the few nearly E-W trending lineaments extracted from the FTG data (Figure 10B) seem to characterize the boundaries of the northern Abaya, southern Abaya and Chamo basins. The NW-SE trending faults reactivated as strike-slip faults that do not significantly affect the morphology of the MER (Chorowicz et al., 1994; Korme et al., 1997; Acocella and Korme 2002), this NW-SE trending faults of the Mesozoic Ogaden aborted rift which is formed by the lower-middle Jurassic reactivations traversed perpendicularly by the Ethiopian Neogene rift forming faults NE-SW structures affecting propagation pattern of Cenozoic rifting (Korme et al., 2004). Thus the relatively deeper source of NW-SE and nearly E-W structures delineated in the northern Abaya, southern Abaya and Chamo basins are associated with the Pre-Tertiary rift structures may be indicative of the presences of Mesozoic sediments in the study area.

Along the length of the rift system continental rift zones comprise a series of discrete and kinematically linked basins (Bosworth 1985; Rosendahl 1987). Fault-bounded sedimentary basins are formed through repeated episodes of faulting, with or without magmatism, over millions of years. So those kinematically linked basins along the southern main Ethiopian rift, that is, northern and southern Abaya, Chamo and Gelana basins may be related to the fault-bounded sedimentary basins that are formed through repeated episodes of faulting.

The depth to the top of the lineaments estimated from the tilt angles (Figure 11A & B) on average varies from 0.9 km to 3.1 km. Most of the shallow depth linear trends are observed in the northern parts and only few shallow depth linear trends are observed on the central where the sub-basins reside. Also the depth to the top of the linear trends observed in the Abaya, Chamo and Gelana basins are relatively deeper compared to the adjacent areas may be related to thick sediment infill of the sub-basins. This interpretation generally agrees with the work of Ebinger et al. (1993), geological cross-sections reconstructed using bedding and fault orientations measured in the field suggest a rather symmetric structure in the Chamo basin, with thickness of syn-rift deposits of ~2 km, and an asymmetric architecture in the Galana basin, with the master fault located on the western side and maximum thickness of the rift infill that may exceed 4 km. Automatic edge detection performed on Tilt Derivative Horizontal (TDX) (Figure 12A) accentuates the traces of the boundaries of the sub basins.

12. Conclusion

In this paper we adapt the tilt angle method with and without a scale value to interpret the FTG data set to delineate the shallow subsurface geology and structural features associated with depth estimation of sediment thickness of southern main Ethiopian rift basin including analysis and interpretations of anomaly maps. The FTGeX instrument that measures the Gravity Gradient Tensor field into five independent components has also made direct measurement of the vertical gravity signal via the Gravity Measurement Assembly (GMA). Thus analysis and interpretation of the Bouguer gravity anomalies are also performed in order to get a better picture of the subsurface geology.

The Bouguer gravity anomaly is analyzed to delineate shallow subsurface geology by extracting the residual gravity value. The behavior of the anomaly signatures fits quite well with the surface geology and with the previous geological studies. The low density Quaternary and Tertiary sedimentary rocks (lacustrine, alluvium, eluvium) as well as Late Cenozoic fluviolacustrine deposits in Abaya, Chamo and Gelana basins are associated with low gravity amplitudes. Local high amplitude in north and upper east of Abaya basin generally corresponds to volcanic rocks. In agreement with the residual gravity anomalies, the vertical gravity gradient clearly outlined the sub-basins with its low gradient amplitude and clearly outlines the boundaries of the sub-basins with high gradient amplitude.

The spatial images of the tilt angle maps reflect the different attributes of linear features, faults, contacts, and edges of the basins and provide the depths estimates of the anomalous bodies. The lineament map prepared using the tilt angle maps confirms the geological results and also identified structures not known before. The analyses performed offering insight about the structures that forms the Abaya, Chamo and Gelana basins. There appears to be no structural connections between the northern and southern Abaya basins, rather the northern Abaya and Gelana basins appear to be formed within the same structure.

The depths to the top of the lineaments were estimated from the tilt angle maps. Most of the shallow depths are observed in the northern parts of the area in comparison to the deeper linear trends that demarcate the boundaries of N&S Abaya, Chamo and Gelana basins. Thickness estimations were also made of the rift infill of the basins.

Declarations

Author contribution statement

Bisrat Kebede: Conceived and designed the experiments; Performed the experiments; Analyzed and interpreted the data; Contributed reagents, materials, analysis tools or data; Wrote the paper.

Tilahun Mammo: Analyzed and interpreted the data; Contributed reagents, materials, analysis tools or data; Wrote the paper.

Funding statement

This research did not receive any specific grant from funding agencies in the public, commercial, or not-for-profit sectors.

Data availability statement

The data that has been used is confidential.

Declaration of interests statement

The authors declare no conflict of interest.

Additional information

No additional information is available for this paper.

References

Abbate, E., Sagri, M., 1980. Volcanites of Ethiopian and Somali plateaus and major tectonic lines. Atti Convegni Lincei 47, 219–227.
Abebe, Tsegaye, 2000. Geological limitations of a geothermal system in a continental rift zone: example the Ethiopian rift valley.. In: Proceedings World Geothermal Congress. Kyushu-Tohoku, Japan, May.
Abebe, Tsegaye, Mazzarini, F., Innocenti, F., Manetti, P., 1998. The yerer-tullu Wellel volcanotectonic lineament: a transtensional structure in Central Ethiopia and the associated magmatic activity. J. Afr. Earth Sci. 26 (1), 135–150.
Acocella, V., Korme, T., 2002. Holocene extension direction along the main Ethiopian rift, East Africa. Terra. Nova 14 (3), 191–197.
Africa Oil Corp, 2013a. ARKeX air FTG® data acquisition report on rift valley basin block, Ethiopia. Unpublished report, ministry of mines and Petroleum, Addis Ababa, Ethiopia. ARX 13501, 1–37.
Africa Oil Corp, 2013b. Corporate Presentation: A Major Emerging Oil Company in East Africa.
Arisoy, Muzaffer Ozgo, Dikmen, U., 2013. Edge detection of magnetic sources using enhanced total horizontal derivative of the tilt angle. Bull. Earth Sci. Appl. Res. Cent. Hacet. Univ. 34 (1), 73–82.
Beiki, Majid, 2010. Analytic signals of gravity gradient tensor and their application to estimate source location. Geophysics 75 (6), I59–74.
Boccaletti, Mario, Bonini, Marco, Mazzuoli, Roberto, Bekele Abebe, Piccardi, Luigi, Tortorici, Luigi, 1998. Quaternary oblique extensional tectonics in the Ethiopian rift (Horn of Africa). Tectonophysics 287 (1–4), 97–116.
Bonini, Marco, Corti, Giacomo, Innocenti, Fabrizio, Manetti, Piero, Mazzarini, Francesco, Tsegaye Abebe, Pecskay, Zoltan, 2005. Evolution of the main Ethiopian rift in the frame of Afar and Kenya rifts propagation. Tectonics 24 (1).
Bosworth, William, 1985. Geometry of propagating continental rifts. Nature 316 (6029), 625–627.
Chorowicz, Jean, Collet, Bernard, Bonavia, Franco F., Korme, Tesfaye, 1994. Northwest to north-northwest extension direction in the Ethiopian rift deduced from the orientation of extension structures and fault-slip analysis. Geol. Soc. Am. Bull. 106 (12), 1560–1570.
Cooper, G.R.J., Cowan, D.R., 2006. Enhancing potential field data using filters based on the local phase. Comput. Geosci. 32 (10), 1585–1591.
Corti, Giacomo, 2009. Continental rift evolution: from rift initiation to incipient break-up in the main Ethiopian rift, East Africa. Earth Sci. Rev. 96 (1–2), 1–53.
Davidson, A., Rex, D.C., 1980. Age of volcanism and rifting in southwestern Ethiopia. Nature 283 (5748), 657–658.
Dickinson, J.L., Murphy, C.A., Robinson, J.W., 2010. Analysing full tensor gravity data with intuitive imaging techniques. In: In 72nd EAGE Conference and Exhibition-Workshops and Fieldtrips. European Association of Geoscientists & Engineers, p. 161.
Dickinson, Jade L., Murphy, Colm A., Robinson, James W., 2012. Interpretation of FTG data using tensor Axis realignment. ASEG Extend. Abst. 2012 (1), 1–2.
Difrancesco, D., 2007. Advances and challenges in the development and deployment of gravity gradiometer systems. In: In EGM 2007 International Workshop. European Association of Geoscientists & Engineers, p. 166.
Ebinger, C.J., Yemane, Tesfaye, Wolde Gabriel, Gidey, Aronson, J.L., Walter, R.C., 1993. "Late eocene–recent volcanism and faulting in the southern main Ethiopian rift. J. Geol. Soc. 150 (1), 99–108.
Ebinger, C.J., Yemane, Tilahun, Harding, D.J., Tesfaye, Samson, Kelley, S., Rex, D.C., 2000. Rift deflection, migration, and propagation: linkage of the Ethiopian and eastern rifts, Africa. Geol. Soc. Am. Bull. 112 (2), 163–176.
Fernandes, R.M.S., Ambrosius, B.A.C., Noomen, R., Bastos, L., Combrinck, L., Miranda, J.M., Spakman, W., 2004. Angular velocities of Nubia and Somalia from continuous GPS data: implications on present-day relative kinematics. Earth Planet Sci. Lett. 222 (1), 197–208.
Gebriel, Tamiru, Seyid, Getahun, Mahari, Kiros, Hassen, Nasir, Samuel, Gichile, Alemu, Tadesse, Yemane, Tesfaye, Genzebu, Woldegabriel, 1997. Geological Map of Agere Mariam Map Sheet (NB37-10), Memoir 8. Geological Survey of Ethiopia, Addis Ababa.
George, Rhiannon, Rogers, Nick, Kelley, Simon, 1998. Earliest magmatism in Ethiopia: evidence for two mantle plumes in one flood basalt province. Geology 26 (10), 923–926.
Ibraheem, Ismael M., Gurk, Marcus, Tougiannidis, Nikolaos, Tezkan, Bülent, 2018. Subsurface investigation of the Neogene mygdonian basin, Greece using magnetic data. Pure Appl. Geophys. 175 (8), 2955–2973.
Jacobsen, Bo Holm, 1987. A case for upward continuation as a standard separation filter for potential-field maps. Geophysics 52 (8), 1138–1148.
Kazmin, V., Berhe, S.M., Walsh, J., 1980. Report on the Geological Map of the Ethiopian Rift Valley. Ethiopian Institute of Geological Survey.
Kebede, Hailemichael, Alemu, Abera, Fisseha, Shimeles, 2020. Upward continuation and polynomial trend analysis as a gravity data decomposition, case study at ziway-shala basin, central main Ethiopian rift. Heliyon 6 (1), e03292.
Korme, Tesfaye, Acocella, Valerio, Abebe, Bekele, 2004. The role of pre-existing structures in the origin, propagation and architecture of faults in the main Ethiopian rift. Gondwana Res. 7 (2), 467–479.
Korme, Tesfaye, Jean, Chorowicz, Collet, Bernard, Bonavia, Franco F., 1997. Volcanic vents rooted on extension fractures and their geodynamic implications in the Ethiopian rift. J. Volcanol. Geoth. Res. 79 (3–4), 205–222.
Le Turdu, Caroline, Jean-Jacques, Tiercelin, Gibert, Elisabeth, Travi, Yves, Lezzar, Kiram-Eddine, Richert, Jean-Paul, Massault, Marc, Gasse, Françoise, Bonnefille, Raymonde, Decobert, Michel, 1999. "The ziway–shala Lake basin system, main Ethiopian rift: influence of volcanism, tectonics, and climatic forcing on basin formation and sedimentation. Palaeogeogr. Palaeoclimatol. Palaeoecol. 150 (3–4), 135–177.
Levitte, Dubi, Columba, John, Mohr, Paul, 1974. Reconnaissance geology of the Amaro horst, southern Ethiopian rift. Geol. Soc. Am. Bull. 85 (3), 417–422.
Lyngsie, Stig Bjarke, Thybo, Hans, Maack Rasmussen, Thorkild, 2006. Regional geological and tectonic structures of the north sea area from potential field modelling. Tectonophysics 413 (3–4), 147–170.
Mahatsente, Rezene, Jentzsch, G., Jahr, T., 1999. Crustal structure of the main Ethiopian rift from gravity data: 3-dimensional modeling. Tectonophysics 313 (4), 363–382.
Mammo, Tilahun, 2010. Delineation of sub-basalt sedimentary basins in hydrocarbon exploration in north Ethiopia. Mar. Petrol. Geol. 27 (4), 895–908.
Mammo, Tilahun, 2013. Crustal structure of the flood basalt province of Ethiopia from constrained 3-D gravity inversion. Pure Appl. Geophys. 170 (12), 2185–2206.
McBarnet, A., 2004. ARKeX on the way to hatching an EGG. First Break 22 (11).
Mengesha, T., Tadiwos, C., Workneh, H., 1996. The Geological Map of Ethiopia, 1: 2,000,000 Scale. EIGS Addis Ababa, Ethiopia.
Mickus, Kevin L., Carlos, L.V., Aiken, Kennedy, W.D., 1991. Regional-residual gravity anomaly separation using the minimum-curvature technique. Geophysics 56 (2), 279–283.
Miller, Hugh G., Singh, Vijay, 1994. "Potential field tilt—a new concept for location of potential field sources. J. Appl. Geophys. 32 (2–3), 213–217.
Mohr, P.A., 1967. The Ethiopian Rift System, Bulletin of the Geophys., 11 Obs. Addis Ababa University.
Montaj, Geosoft Oasis, 2015. Data Processing and Analysis Systems for Earth Science Applications. Geosoft Inc, Toronto, Canada (Ver. 8.3. 3).
Murphy, C.A., 2007. Interpreting FTG gravity data using horizontal tensor components. In: EGM 2007 International Workshop.
Murphy, C.A., Dickinson, J.L., 2010. Geological mapping and targeting using invariant tensor analysis on full tensor gravity data. In: EGM 2010 International Workshop.
Murphy, Colm A., 2004. The air-FTG airborne gravity gradiometer system. Airborne Gravity 7–14.
Murphy, Colm A., Brewster, James, 2007. Target delineation using full tensor gravity gradiometry data. ASEG Extend. Abst. 2007 (1), 1–3.
Murphy, Colm A., Mumaw, Gary R., Karel, Zuidweg, 2005. Regional target prospecting in the faroe-shetland basin area using 3D-FTG gravity data. In: 67th EAGE Conference & Exhibition. European Association of Geoscientists & Engineers, p. 1.
Rosendahl, Bruce R., 1987. Architecture of continental rifts with special reference to East Africa. Annu. Rev. Earth Planet Sci. 15 (1), 445–503.
Salem, A.S.K., Campell, S., Derek, J.D., Dickinson, J., Murphy, C., 2011. Interpretation of tensor gravity data using an adaptive tilt angle technique. In: 73rd EAGE Conference and Exhibition Incorporating SPE EUROPEC 2011. European Association of Geoscientists & Engineers, p. 238.
Salem, Ahmed, Williams, Simon, Fairhead, J Derek, Ravat, Dhananjay, Smith, Richard, 2007. Tilt-depth method: a simple depth estimation method using first-order magnetic derivatives. Lead. Edge 26 (12), 1502–1505.
Sickenberg, O., Schönfeld, M., 1975. "The Chorora Formation—lower Pliocene limnical sediments in the southern Afar (Ethiopia)." in *Afar Depression of Ethiopia*. E. Schweizerbartsche Verlagsbuchhandlung Stuttgard 1, 277–284.
Tiercelin, J.-J., Lezzar, K.-E., 2002. A 300 million years history of rift lakes in central and east Africa: an updated broad review. In: The East African Great Lakes: Limnology, Palaeolimnology and Biodiversity, 3–60. Springer.

Woldegabriel, Giday, Aronson, James L., Walter, Robert C., 1990. Geology, geochronology, and rift basin development in the central sector of the main Ethiopia rift. Geol. Soc. Am. Bull. 102 (4), 439–458.

WoldeGabriel, Giday, Yemane, Tesfaye, Gen, Suwa, White, T., Asfaw, Berhane, 1991. Age of volcanism and rifting in the burji-soyoma area, Amaro horst, southern main Ethiopian rift: geo-and biochronologic data. J. Afr. Earth Sci. 13 (3–4), 437–447.

Yemane, T., WoldeGabriel, G., Tesfaye, S., Berhe, S.M., Durary, S., Ebinger, C., Kelley, S., 1999. Temporal and geochemical characteristics of tertiary volcanic rocks and tectonic history in the southern main Ethiopian rift and the adjacent volcanic fields. Acta Vulcanol. 11, 99–120.

Yismaw, Aman., Mitiku, Bezayit., Beyene, Birhanu., G/Tsadik, Tesfay, Dure, Tarekegn., Zwde, Teferi., Theshome, Yonas., Tesfaye, Weynu., Abraham, Rahel, 2015. Geological Map of Dilla Map Sheet (NB37-6), Memoir 37. Geological Survey of Ethiopia, Addis Ababa.